

establish initial convergence, the primary control system was engaged and a series of inputs was applied to demonstrate the performance of the adaptation logic. The pilot was not given an indication of angle of bank during the run. This resulted in a rolling supersonic dive ($M=1.03$). The altitude transition during the run was from 20 000 to 8000 ft. As in the longitudinal case, the performance of the adaptive system can be observed during the time intervals when the system is engaged. The uniformity of the roll rate response during engagement can be observed by comparing the steady-state roll rate at 20, 60, 80, and 100 s. Note the variability of the steady-state roll rate during time intervals where the primary control system is not engaged (e.g., at 5, 40, and 120 s). Note also that the surface commands required to realize the uniform roll rate responses vary considerably during the run. During the run, inputs were also made in rudder to examine the dutch roll adaptation characteristics. The dutch roll mode is observed to maintain a 0.7 damping ratio by examining the sideslip angle response to rudder inputs at times of 30, 63, 83, and 110 s. These can be compared with the unaugmented responses at 10 and 50 s.

IV. CONCLUSIONS

This paper describes the moving window adaptive control concept which has been developed as a candidate for flight test on the NASA F8-DFBW aircraft. Included are studies of the effects of auxiliary dither inputs to aid identification, data base size, measurement noise, and other design considerations. Results were presented indicating the performance of the system in a nonlinear six-degree-of-freedom simulation of an F-8C aircraft. This study has shown that when there is sufficient

motion of the aircraft, the adaptive algorithm converges to a linear mathematical model of the aircraft. Furthermore, it was shown that once these parameters have passed specified convergence criteria they may be used in an algebraic calculation of feedback and feedforward gains which satisfy certain flying quality requirements. Extensive simulation studies must be made before the moving window parameter adaptive control system can be recommended for flight test; however, results presented here indicate that the system is promising and should be evaluated further. One item requiring further evaluation and possible modification is the suitability of the mode of operation of the process without dither.

REFERENCES

- [1] J. R. Elliott, "NASA's advanced control law program for the F-8 digital fly-by-wire aircraft," this issue, pp. 753-757.
- [2] J. L. Picon, "Design of a digital adaptive control system for atmospheric reentry vehicles," Ph.D. dissertation, Virginia Polytechnic Inst. and State Univ., Blacksburg, Oct. 1971.
- [3] F. H. Schlee, C. T. Standish, and N. F. Toda, "Divergence in the Kalman filter," *AIAA J.*, vol. 5, pp. 1114-1120, June 1967.
- [4] A. H. Jazwinski, "Limit memory optimal filtering," *IEEE Trans. Automat. Contr.*, vol. AC-13, pp. 558-563, Oct. 1968.
- [5] N. K. Gupta and R. K. Mehra, "Computational aspects of maximum likelihood estimation and reduction in sensitivity function calculation," *IEEE Trans. Automat. Contr.*, vol. AC-19, pp. 774-783, Dec. 1974.
- [6] R. K. Mehra, "Optimal input signals for parameter estimation in dynamic systems—Survey and new results," *IEEE Trans. Automat. Contr.*, vol. AC-19, pp. 753-769, Dec. 1974.
- [7] C. R. Chalk and R. K. Wilson, "Airplane flying qualities specification revision," *AIAA J. Aircraft*, vol. 6, pp. 232-240, May-June 1969.
- [8] C. T. Woolley, "A real-time hybrid simulation of a digital fly-by-wire aircraft," presented at the 1974 Summer Computer Simulation Conf., Houston, TX, July 9-11, 1974.

F-8 DFBW Sensor Failure Identification Using Analytic Redundancy

JAMES C. DECKERT, MEMBER, IEEE, MUKUND N. DESAI, MEMBER, IEEE,
JOHN J. DEYST, MEMBER, IEEE, AND ALAN S. WILLSKY, MEMBER, IEEE

Abstract—In this paper, we outline the structure of a sensor failure detection and identification system designed for the NASA F-8 DFBW aircraft. The system is for use in a dual-redundant environment, and it takes maximal advantage of all functional relationships among the sensed variables. The identification logic uses the quality sequential probability ratio, which provides a useful on-line measure of confidence in the various forms of analytic redundancy. Preliminary simulation results indicate good behavior of the analytic decision statistic, based on the sequential probability ratio test.

LIST OF SYMBOLS

A Vector of ideal accelerometer outputs.
 A' Vector of ideal accelerometer outputs compensated for lever-arm effects.
 B Instrument failure bias assumed by an individual SPRT.
 C_m Measured unit vector coefficient for gravity in aircraft axes.
 D Aerodynamic drag.

F Vector of aerodynamic forces on aircraft.
 G_k Translational kinematics SPRT gain factor at time t_k .
 g Acceleration of gravity.
 h Altitude.
 k Filter gain.
 L Aerodynamic lift.
 M Mach number.
 m Aircraft mass.
 m_k Hypothesized mean in γ_k due to sensor failure.
 N Number of samples in residual window.
 N_p Number of passes allowed through identification logic.
 p Roll rate, defined about aircraft longitudinal (x) axis.
 q Pitch rate, defined about aircraft lateral (y) axis.
 \bar{q} Dynamic pressure.
 r Yaw rate, defined about aircraft normal (z) axis.
 S Aircraft wing area.
 T Engine thrust.
 t_n Arbitrary instant of time.
 u_n Output of SPRT at time t_n .
 V Velocity of aircraft with respect to the air mass.
 V_s Velocity of sound.
 Y Aerodynamic sideforce.
 α Angle of attack.
 β Sideslip angle.

Manuscript received June 3, 1976; revised October 1, 1976. This work was supported by the NASA Langley Research Center under Contract NAS1-13914.

J. C. Deckert, M. N. Desai, and J. J. Deyst are with the Charles Stark Draper Laboratory, Inc., Cambridge, MA 02139.

A. S. Willsky is with the Department of Electrical Engineering and Computer Science, Massachusetts Institute of Technology, Cambridge, MA 02139.

γ_k	Input to SPRT at time t_k .
δ_a	Aileron position.
δ_e	Elevator position.
δ_r	Rudder position.
θ	Euler pitch angle.
ξ	Inertial acceleration of air mass.
σ^2	Variance of the observation of γ_k .
ϕ	Euler roll angle.
ψ	Euler yaw angle.
Ω	Skew-symmetric cross-product matrix.
Boldface	Vector quantity.

Superscripts

'	Time derivative.
^	Estimated quantity.
-	Averaged quantity.

Subscripts

m	Measured quantity.
1,2	Relative to instrument 1 or 2 of a given type.

I. INTRODUCTION

The goal of the research reported in this paper is a system for the detection and identification of sensor failures in the NASA F-8 digital fly-by-wire (DFBW) aircraft. In particular, the research is aimed at devising relatively sophisticated detection mechanisms that are capable of operating in an environment without triple redundancy. Thus, a basic ground rule for the work presented in this paper is the development of tests that can make decisions based on information from dissimilar instruments.

In recent years, a number of techniques have been proposed for the detection of system failures [1]-[16].¹ Many of these techniques deal with the utilization of analytic redundancy among dissimilar instruments, in which one uses knowledge of the functional relationships among the variables being measured by the various sensors. However, despite the sophistication of these methods, it is fair to say that these analytic redundancy techniques are all at a relatively early stage of development, and each of them can be criticized for computational complexity greatly exceeding the on-board computer constraints present in the F-8 problem. Given these constraints, we have developed the following philosophy for the development of our failure detection and identification (FDI) system:

1) We work with a dual-redundant system. This allows a direct comparison between pairs of like instruments to detect failures and leads to two important advantages:

a) One can use this direct comparison to detect failures and thus need rely on analytic redundancy only for identifying which of the two instruments has failed. In such a mode, the analytic redundancy test can be made more robust.

b) One can use the direct test to trigger the somewhat more complex analytic redundancy tests. Such a dual-mode procedure greatly reduces the average computational load. Additionally, we may initiate the analytic redundancy tests in the absence of a direct redundancy trigger to identify changes that affect like instruments in the same way (e.g., thermal effects on sensors mounted in the same part of the aircraft).

2) For each sensor, we determine several kinematic and dynamic relationships between the given instrument and other instruments. The object here is:

a) To determine a number of independent tests that can be used to check the correctness of a given instrument, thus extracting the maximal amount of information concerning each instrument.

b) To develop comparison tests that are relatively simple to implement and robust in the presence of unmodeled effects.

3) We limit ourselves to looking for bias failures. The reasons for this are:

a) Although descriptions of actual failure modes were not available, it was felt that biases were a likely failure mode.

b) Techniques looking for bias failures can often find other types of failures.

c) The algorithms in this case are extremely simple to implement.

In the remainder of this paper we describe our design methodology in detail, outlining how we have met the various design constraints and developing several fundamental design concepts that we feel are of importance. In addition, we have made an effort to indicate the assumptions underlying our approach and the limitations on its performance, together with possible modifications that can deal with these. The organization of the paper is as follows. In Section II, we outline the structure of the dual-mode FDI system (direct comparison trigger followed by analytic redundancy identification), indicating the various types of analytic redundancy available and also introducing the analytic decision statistic which is based on the *sequential probability ratio test* (SPRT, [17]). In Section III, we describe, in detail, the various SPRT tests for all of the F-8 sensors, while in Section IV, we present and discuss some simulation results that indicate the characteristics of our design. In Section V, we discuss the choice of system parameters and the *quality sequential probability ratio* (QSPR), which is computed on-line and provides a measure of confidence in its associated analytic redundancy test. We also briefly discuss the outer loop logic which must interpret the various direct and analytic decision statistics and make a decision. One attribute of this logic is that it can make provisional decisions and can seek further corroboratory information. This approach minimizes decision time without sacrificing performance in the form of high false alarm rates. Finally, in Section VI, we summarize the paper and make some concluding remarks.

II. FDI STRUCTURE

The FDI for an instrument type with dual redundancy is accomplished in two steps. First, the failure of one instrument of the pair is detected by examining only the dual instrument readings. Subsequent to the detection of a failure, several SPRT's are initiated utilizing the direct redundancy and all possible analytic redundancy between the failed instrument type and the other instrument types. The identification of which instrument of the pair has failed, or the indication of a false alarm, is accomplished via logical processing of the various SPRT's as discussed in Section V.

A. Detection

A direct redundancy detector, called a *redundancy trigger*, operates on the moving window average of the output of instrument 1 minus the output of instrument 2 for each instrument type. A *bias failure magnitude* (BFM) is defined for each instrument type based on both the *a priori* sensor statistics and the capabilities of the various analytic redundancy failure identification techniques in the presence of allowable errors on *unfailed instruments*. A *threshold magnitude* and *window size* are chosen for each instrument type to give reasonable false alarm and missed alarm probabilities, where a false alarm is the indication of a bias when in fact a bias of half the BFM magnitude or larger is not present, and a missed alarm is the failure to detect the presence of a bias of magnitude larger than the defined BFM. If the redundancy trigger detects a significant mean in the moving window average of the output of instrument 1 minus the output of instrument 2, it follows that if the sign of this mean is positive (negative) either instrument 1 has a positive (negative) bias or instrument 2 has a negative (positive) bias. This failure sign information halves the number of SPRT's required for failure identification in dual redundant instruments.

B. Identification Using SPRT's

Following the detection of the failure of one instrument of a given type by the redundancy trigger, several SPRT's are initiated to identify

¹See the survey paper [1] for further references and brief descriptions and comparisons of some of these methods.

which of the two instruments of the given type has failed. A brief introduction to the SPRT will now be presented, and the reader is referred to [17], [18] for a full theoretical development.

As implemented in this study, the SPRT makes sequential observations of the process γ , which represents a comparison between the suspect instrument and other unfailed instrument types.² The sample from the process γ at time t_k is called γ_k . The SPRT gathers enough information to choose between the two hypotheses:

- H_1 : at time t_k , the process γ is Gaussian with mean m_k and covariance P
 H_2 : at time t_k , the process γ is Gaussian with mean $\mathbf{0}$ and covariance P

where H_1 is the failure hypothesis and H_2 is the no-failure hypothesis. The log likelihood ratio for the k th sample is defined as

$$z_k = -\ln \frac{p(\gamma_k|H_1)}{p(\gamma_k|H_2)} \quad (2.2-1)$$

and after n samples have been taken (assuming the independence of the γ 's), the log likelihood ratio of the n samples is given by

$$u_n = -\ln \frac{p(\gamma_1, \dots, \gamma_n|H_1)}{p(\gamma_1, \dots, \gamma_n|H_2)} = \sum_{k=1}^n z_k \quad (2.2-2)$$

For the case of the two hypotheses given above, the form of z_k is given by

$$z_k = \left(\frac{m_k}{2} - \gamma_k \right)^T P^{-1} m_k \quad (2.2-3)$$

and the log likelihood ratio for n samples given by (2.2-2) becomes

$$u_n = \sum_{k=1}^n \left(\frac{m_k}{2} - \gamma_k \right)^T P^{-1} m_k \quad (2.2-4)$$

Assuming that either H_1 or H_2 is true, the stipulation of incorrect classification probabilities directly yields (see [18]) the thresholds $a < 0$ and $b > 0$ and the following decision rule:

$$\begin{aligned} u_n \leq a, & \quad \text{accept } H_1 \\ a < u_n < b, & \quad \text{take another sample} \\ b \leq u_n, & \quad \text{accept } H_2. \end{aligned} \quad (2.2-5)$$

If the log likelihood ratio is between the thresholds, a choice of hypotheses cannot yet be made which meets the specified incorrect classification probabilities, and another sample must be taken.

One attractive property of the SPRT is that it minimizes the average number of observations necessary to meet these probabilities. In addition, the SPRT is independent of the *a priori* probabilities of the two hypotheses. It is because of these properties of the SPRT and because of its inherent simplicity as shown in (2.2-4) and (2.2-5) that the SPRT was chosen as the basic identification tool for this study. A further simplification follows since all of the observed processes in this work are chosen to be scalar or the sum of scalars. The scalar form of (2.2-4) is given by

$$u_n = \frac{m_k}{\sigma^2} \sum_{k=1}^n \left(\frac{m_k}{2} - \gamma_k \right) \quad (2.2-6)$$

where σ^2 is the variance of the scalar process γ . Observe that if the mean m_k is present in γ_k , the expected value of u_n is

$$E\{u_n\} = \frac{1}{2\sigma^2} \sum_{k=1}^n (-m_k^2) \quad (2.2-7)$$

In fact, any mean of γ_k with the sign of m_k and greater in magnitude than $|m_k|/2$ will drive u_n toward the negative threshold, which by our definition indicates an instrument failure. Thus an individual SPRT may make a false indication unless the mean m_k is chosen such that biases in instruments operating within tolerance have magnitude less than $|m_k|/2$.

Following the detection of a failure by the redundancy trigger, several SPRT's are begun. One direct redundancy SPRT observes the difference between instrument 1 and instrument 2 of the detected failure type, the same process observed by the redundancy trigger. The mean which constitutes the failure hypothesis m_k has magnitude equal to the predefined sensor BFM and has the sign of the moving window average computed by the trigger. This SPRT serves to corroborate the trigger concerning the presence of a difference between the two instruments.

Additionally, one SPRT for each instrument of the failed type is begun for every kind of analytic redundancy available. Detailed descriptions of these tests are given in the next section. The underlying basis for the analytic redundancy SPRT's is the comparison of the measurement of a variable obtained using the suspect instrument and another measurement of the same variable obtained using other instrument types. The difference in these measurements forms the residual γ_k which is the input to the SPRT. The mean for each SPRT, m_k , is calculated to be consistent with the predefined sensor BFM and the failure sign information from the redundancy trigger.

Finally, one QSPR calculation is started for every kind of analytic redundancy available. The QSPR is a measure of the signal-to-noise ratio of its associated analytic redundancy tests, and is used in the failure identification logic discussed in Section V.

III. ANALYTIC REDUNDANCY SPRT'S

The dual redundant instrument types which are available on the F-8 DFBW aircraft are the following: longitudinal accelerometer, lateral accelerometer, normal accelerometer, roll rate gyro, pitch rate gyro, yaw rate gyro, vertical gyro, directional gyro, altimeter, Mach meter, and alpha vane. In addition, a nonredundant beta vane is available. Each vertical gyro gives an indication of pitch angle θ and roll angle ϕ . In this paper, only the failures of the dual redundant instrument types are addressed, and failures of the indication of θ and ϕ for each vertical gyro are considered to be independent. The consideration of simultaneous failures of both of these measurements will be investigated in the future.

Three types of analytic redundancy are utilized in this study: translational kinematics redundancy exists between the integrated output of the accelerometers, vertical gyros, and rate gyros and the outputs of the air data sensors, i.e., the Mach meter, altimeter, and alpha and beta vanes. Translational dynamics redundancy relates the aerodynamic forces on the aircraft measured by the accelerometers and the calculated aerodynamic forces based on the air data sensors through stored aerodynamic coefficients. Rotational kinematics redundancy relates the integrated outputs of the rate gyros and the outputs of the vertical and directional gyros. In the following subsections, these three types of analytic redundancy and the SPRT's exploiting them will be discussed in detail.

A. Translational Kinematics

The translational kinematics SPRT's utilize the redundant information concerning the translational motion of the aircraft. The body-mounted linear accelerometers measure the body axis components of the non-gravitational contribution to the acceleration of the aircraft with respect to inertial space. The measured velocity V_m is the noisy measurement of the velocity V of the aircraft with respect to the air mass expressed in body axes. This air-relative velocity vector is a function of Mach number M , angle of attack α , sideslip angle β , and the speed of sound V_s , which is itself a function of the altitude h :

$$V = \begin{bmatrix} \cos \beta \cos \alpha \\ \sin \beta \\ \cos \beta \sin \alpha \end{bmatrix} V_s(h) M. \quad (3.1-1)$$

The differential equation for the air-relative velocity is given by

²The details of this process for the various instruments on the F-8 are presented in Section III.

$$\dot{\hat{V}} = \frac{1}{m}F + g - \Omega V - \xi \quad (3.1-2)$$

where m is the aircraft mass, F is the aerodynamic force on the aircraft, and g is the gravity vector. The matrix Ω is the skew-symmetric cross-product matrix

$$\Omega = \begin{bmatrix} 0 & -r & q \\ r & 0 & -p \\ -q & p & 0 \end{bmatrix} \quad (3.1-3)$$

where p , q , and r are the roll rate, pitch rate, and yaw rate, respectively. The vector ξ is the acceleration of the air mass with respect to inertial space. Assuming that the accelerometers are located at the same position R away from the center of mass, the vector A composed of the outputs of ideal x , y , and z accelerometers is related to the aerodynamic force via

$$A = \frac{1}{m}F + [\Omega^2 + \dot{\Omega}]R. \quad (3.1-4)$$

The compensated ideal accelerometer output vector A' is defined as

$$A' = A - [\Omega^2 + \dot{\Omega}]R. \quad (3.1-5)$$

Equations (3.1-2), (3.1-4), and (3.1-5) yield

$$\dot{\hat{V}} = A' + g - \Omega V - \xi. \quad (3.1-6)$$

The translational kinematics SPRT's utilize the following discrete approximation to (3.1-6) to propagate the air-relative velocity estimate \hat{V} ahead one time step:

$$\hat{V}'(t_n) = \hat{V}(t_{n-1}) + \{ \bar{A}'_m + \bar{C}_m g - \bar{\Omega}_m \bar{V}_m \} [t_n - t_{n-1}]. \quad (3.1-7)$$

The measured air-relative velocity is incorporated into the estimate via

$$\hat{V}(t_n) = \hat{V}'(t_n) + k\gamma(t_n) \quad (3.1-8)$$

where

$$\gamma(t_n) = V_m(t_n) - \hat{V}'(t_n). \quad (3.1-9)$$

The inputs to the translational kinematics SPRT's are the components of the measurement residual vector $\gamma(t_n)$. In (3.1-7) a bar over a variable indicates that it is averaged over the interval (t_{n-1}, t_n) , an m subscript indicates a measured quantity, and the prime on $\hat{V}'(t_n)$ indicates that it is the propagated estimate not including the present measurement. The vector \bar{A}'_m indicates the average of the compensated accelerometer outputs at t_n and t_{n-1} . The compensation equation given by (3.1-5) is utilized, with the $\bar{\Omega}$ terms obtained as the differences of the respective rate gyro outputs at times t_n and t_{n-1} divided by the time step, and the $\bar{\Omega}$ terms being the averages of those rate gyro outputs. The vector \bar{C}_m is obtained using the average of the vertical gyro measurements of ϕ and θ over the interval

$$\bar{C}_m = \begin{bmatrix} -\sin \bar{\theta}_m \\ \cos \bar{\theta}_m \sin \bar{\phi}_m \\ \cos \bar{\theta}_m \cos \bar{\phi}_m \end{bmatrix}. \quad (3.1-10)$$

The matrix $\bar{\Omega}_m$ uses the averages of the rate gyro outputs. It is also used in the accelerometer compensation equations. The vector \bar{V}_m in (3.1-7) likewise denotes the measured air-relative velocity based on the average of the air data sensor outputs at time t_n and t_{n-1} .

There are three important aspects of the form of (3.1-7):

1) The term in braces indicates an estimate of the air-relative acceleration of the aircraft at the midpoint of the propagation interval, and the resulting integration rule is good to approximately second order. This second-order integration rule is used to ensure accurate filter performance during high rate or acceleration maneuvers.

2) The average measured velocity is used in the right-hand side of (3.1-7). Although the standard form of the extended Kalman filter for

this system [19] would employ the estimate \hat{V} , we have chosen to use the average measured velocity derived from air data to decouple the three components of \hat{V} . This decoupling allows the use of scalar SPRT's which will be discussed presently.

3) There is no term in (3.1-7) corresponding to the acceleration of the air mass ξ . Since the effect of a constant value of ξ , i.e., wind shear, is indistinguishable from the effect of an accelerometer bias on the residual process γ , our interpretation of a nonzero component of γ must account for the possibility of wind shear. This idea will be expanded upon shortly.

Assuming that we are interested in identifying bias errors in the sensors, it is clear from (3.1-7) that at least three types of sensor biases will appear as acceleration errors in the propagation equation for \hat{V} :³

- 1) accelerometer biases through \bar{A}'_m
- 2) vertical gyro biases through \bar{C}_m
- 3) rate gyro biases through $\bar{\Omega}_m \bar{V}_m$.

Thus, translational kinematics SPRT's are started when the failure of an accelerometer, vertical gyro, or rate gyro is detected by the trigger. In order to avoid the transient effects of air data sensor noise, one set of equations (3.1-7)–(3.1-9) is always running to provide the initial velocity estimates for the SPRT's. The structures of the SPRT's for all of these instrument types are analogous. Two versions of the filter given by (3.1-7)–(3.1-9) are implemented, one version using the output of the number 1 instrument of the detected failure type, plus all the necessary measurements from the other instrument types, and the other version using the same information with the exception that it uses the output of the number 2 instrument of the detected failure type. The residual process γ from the filter using instrument number 1 (2) is the input process sampled by the SPRT looking for the effect of a bias in instrument number 1 (2). The expected error in acceleration used in the SPRT varies at each sample and is obtained from (3.1-7) using the predefined sensor BFM and the sign of the difference between instruments 1 and 2 as given by the redundancy trigger.

In order to decrease identification times and minimize computational complexity, the translational kinematics SPRT's use a zero value for the gain k in (3.1-8). Thus, the time-varying mean m_k for each SPRT is simply incremented at each sample by the expected velocity error using the assumed sensor bias failure via (3.1-7). For the case of a constant vehicle state and a sensor bias error, the means for the two SPRT's are of opposite sign and grow in magnitude linearly with time. We note that for an accelerometer bias, the resulting velocity error shows up only in the corresponding residual component, allowing the implementation of scalar SPRT's. For rate gyro failures, the corresponding acceleration bias, arising from the ΩV term, leads to a velocity error *essentially* in one component. This is exact when α and β are zero, and the unidirectional assumption is justified for reasonable angles of attack and sideslip. Hence we can also implement scalar SPRT's in this case.

Examination of (3.1-7) is instructive for determining the sizes of biases in the various instruments which can be identified with this technique. Recall that it is highly unlikely that a mean will be indicated by the SPRT if the actual mean present in the process is less than half the mean of the test. Thus, the sum of the acceleration errors due to the acceptable biases in all other instruments used in (3.1-7) must be less than half the SPRT mean for the instrument type being checked, or a false identification may be made. By carefully setting the BFM's for the various instruments in all SPRT's in a consistent manner, the problem of false identification from undetected sensor biases can be minimized.

The remaining factor which can contribute to false identification in the translational kinematics SPRT's is wind shear. Simulations at Mach 0.6 at 20000-ft altitude with a modified Dryden wind model [20] using a 99-percent sigma value of 18 ft/s and a correlation length of 1750 ft have produced wind shears of 10 ft/s² which persist for as long as 6 s. We have found an effective way to minimize erroneous failure identification due to wind shears is to slow down the translational kinematics

³Mach meter failures may be detected by translational kinematics in a manner analogous to that discussed in Section III-A for the attitude sensors using rotational kinematics.

SPRT's. This is done by replacing the gain in the SPRT in (2.2-6), formerly $m_k/(\sigma^2)$, by $G_k/(\sigma^2)$ where G_k and σ^2 reflect the turbulence level, and the gain G_k is held constant beyond a certain time after the start of the SPRT.

To summarize, the translational kinematics SPRT's may be used to identify failures in the accelerometers, the rate gyros, and the vertical gyros. Failures of these instruments manifest themselves as acceleration errors in the equation for the air-relative velocity of the aircraft. Translational kinematics SPRT's for each instrument type look for time-varying means in a component of the velocity filter residual. The levels of detectable sensor biases are functions of the errors arising from allowable biases on unfailed instruments and unmodeled effects.

B. Translational Dynamics

The translational dynamics SPRT's utilize the redundant information related to the aerodynamic forces on the aircraft. The accelerometers measure these aerodynamic forces together with the lever arm forces arising from the fact that the instruments are not located at the vehicle center of mass. In particular, A' , the vector of ideal x , y , and z accelerometer outputs corrected for lever arm effects, is related to the vector of aerodynamic forces on the vehicle F via

$$A' = \frac{1}{m} F. \quad (3.2-1)$$

Vector F may be written as

$$F = \begin{bmatrix} T - D \cos \alpha + L \sin \alpha \\ Y \\ -D \sin \alpha - L \cos \alpha \end{bmatrix} \quad (3.2-2)$$

with L the lift, D the drag, Y the sideforce, and T the engine thrust.

If the aircraft has no flap, leading edge, or speed brake extensions, the lift, drag, and sideforce are given by

$$\begin{aligned} L &= C_L \bar{q} S \\ D &= (C_D + C_{D\delta_r}) \bar{q} S \\ Y &= (C_{y\beta} \beta + C_{y\delta_r} \delta_r + C_{y\delta_a} \delta_a) \bar{q} S \end{aligned} \quad (3.2-3)$$

where the sideforce equation neglects small terms due to roll and yaw rates. In (3.2-3), S is the wing area, \bar{q} the dynamic pressure, δ_r the rudder position, and δ_a the aileron position. The aerodynamic coefficients in (3.2-3) have been determined experimentally and tabulated as functions of Mach, angle of attack, and elevator position. In addition, thrust has been tabulated as a function of air-relative velocity, altitude, and throttle position. By utilizing these tables, or functional approximations to these tables, expected accelerometer outputs can be calculated based on the air data sensors, providing analytic redundancy.

The translational dynamics SPRT's are used to identify failures in the accelerometers, alpha vanes, and Mach meters.⁴ In the case of an accelerometer failure, after detection by the redundancy trigger the calculation of two SPRT's is begun, one for each of the accelerometers of the detected failure type. The input to each SPRT is the respective compensated accelerometer output minus the expected accelerometer output based on the air data measurements. As in the case of the translational kinematics SPRT's, these calculations are made for the midpoint of the sample interval using average sensor outputs. Each SPRT mean is calculated using the predefined accelerometer BFM and the sign information from the redundancy trigger. These mean calculations are performed only when the SPRT's are started and are held constant thereafter.

For the case of an alpha vane or Mach meter detected failure, the procedure is analogous to that outlined above though somewhat more complicated. Two SPRT's are calculated, each using identical air data output, except for the detected failure type, to compute the expected lift

and drag on the vehicle. Each of the two SPRT's uses a different member of the pair of instruments for which a failure has been detected to make these calculations. The expected compensated x and z accelerometer outputs using these two sets of air data sensors are then computed using (3.2-1)–(3.2-3). These two sets of expected compensated x and z accelerometer outputs are then used to calculate the x and z acceleration gradients with respect to the detected failure type. Then the x and z means for the two SPRT's are calculated using the computed gradients, the predefined alpha or Mach BFM, and the sign information from the redundancy trigger. The input to each SPRT consists of a two-dimensional vector of the expected minus the actual x and z accelerometer output. The noises in the two components of this vector are assumed to be uncorrelated with equal variance σ^2 to facilitate computation. To be specific, assume that an alpha vane failure has been detected by the redundancy trigger. Using alpha vane 1 and the other air data sensor types, expected compensated x and z accelerometer outputs $a_{x,1}$ and $a_{z,1}$ are calculated via (3.2-1)–(3.2-3), with expected outputs $a_{x,2}$ and $a_{z,2}$ calculated using alpha vane 2 and the same set of other air data. Assuming that the predefined alpha vane BFM is b_α and the sign of $(\alpha_1 - \alpha_2)$ is s_α from the redundancy trigger, the means for the SPRT using alpha vane 1 are

$$m_{x,1} = \frac{a_{x,1} - a_{x,2}}{\alpha_1 - \alpha_2} b_\alpha s_\alpha \quad (3.2-4)$$

$$m_{z,1} = \frac{a_{z,1} - a_{z,2}}{\alpha_1 - \alpha_2} b_\alpha s_\alpha$$

while the means for the SPRT using alpha vane 2 are

$$m_{x,2} = -m_{x,1} \quad (3.2-5)$$

$$m_{z,2} = -m_{z,1}$$

With the actual compensated accelerometer outputs given by A'_x and A'_z , the SPRT variable u for alpha vane 1 is incremented by

$$\Delta u_1 = \left[\left(\frac{m_{x,1}}{2} - a_{x,1} + A'_x \right) m_{x,1} + \left(\frac{m_{z,1}}{2} - a_{z,1} + A'_z \right) m_{z,1} \right] / \sigma^2 \quad (3.2-6)$$

while the increment for the SPRT using alpha vane 2 is

$$\Delta u_2 = \left[\left(\frac{m_{x,2}}{2} - a_{x,2} + A'_x \right) m_{x,2} + \left(\frac{m_{z,2}}{2} - a_{z,2} + A'_z \right) m_{z,2} \right] / \sigma^2 \quad (3.2-7)$$

The means given by (3.2-4)–(3.2-5) are calculated at each sample using sensor outputs averaged over the interval.

The two major sources of error in the translational dynamics SPRT's involve the aerodynamic coefficients in (3.2-3). One error is the difference between the polynomial approximations to the coefficients, used in the flight computer, and the tabulated values of the coefficients. The impact of this error source can be minimized by the proper choice of fitting functions and by forcing the best fits in the most common flight regions. When the aircraft is flying outside the region of good fit, appropriate increases in the assumed test error must be made to avoid erroneous failure identification. The second error source is the difference between the tabulated aerodynamic coefficients, which reflect our *a priori* knowledge, and the true coefficients for the aircraft. It is felt that the tabulated coefficients have the correct shape but are biased. The evaluation of the effects of the polynomial approximation errors and table bias errors awaits the analysis of actual flight data to be carried out in the future.

C. Rotational Kinematics

In this section, we consider failure identification for the angular sensors, the rate gyros, and attitude gyros, using the kinematic relationship between the angular rate and the attitude of the aircraft.

The body mounted gyros provide noisy measurements p_m , q_m , r_m of the rigid body rates p , q , r about the longitudinal, lateral, and normal body axes, respectively. The attitude sensors, directional and vertical gyros, provide the measurements ψ_m , θ_m , ϕ_m of the Euler angles ψ , θ , ϕ , which define the orientation of the body axes with respect to the

⁴Recall, since we have only a single β vane, we have not considered FDI for this instrument. However, straightforward modification of the analytic redundancy SPRT calculations, described in [9], allows failure identification for single sensors.

navigation frame. The order of the three rotations involved in going from the navigation frame to the body frame is yaw (ψ), pitch (θ), and roll (ϕ).

The rigid body rates p , q , and r are related to the Euler angles and their rates via the relationships [21]

$$\begin{aligned} p &= \dot{\phi} - \dot{\psi} \sin \theta \\ q &= \dot{\theta} \cos \phi + \dot{\psi} \cos \theta \sin \phi \\ r &= -\dot{\theta} \sin \phi + \dot{\psi} \cos \theta \cos \phi. \end{aligned} \quad (3.3-1)$$

The inverse relationships expressing the Euler angle rates in terms of the rigid body rates can be obtained from the above equations to yield

$$\begin{aligned} \dot{\phi} &= p + q \sin \phi \tan \theta + r \cos \phi \tan \theta \\ \dot{\theta} &= q \cos \phi - r \sin \phi \\ \dot{\psi} &= q \sin \phi \sec \theta + r \cos \phi \sec \theta. \end{aligned} \quad (3.3-2)$$

Equations (3.3-2) are not convenient to use to obtain the Euler angle rates from the rigid body rates because of the singularities at $\theta = \pm \pi/2$. Alternate approaches which avoid this singularity involve the differential relationships between elements of the direction cosine matrix or attitude quaternion and the rigid body rotation rates. However, the attendant computational complexity of these approaches may be avoided for the purpose of failure identification by the following set of equations [easily derived from (3.3-1) and (3.3-2)] which also avoids the singularity

$$\begin{aligned} \dot{\phi} &= p + \dot{\psi} \sin \theta \\ \dot{\theta} &= q \cos \phi - r \sin \phi \\ \dot{\psi} &= (\dot{\phi} - p) \sin \theta + (q \sin \phi + r \cos \phi) \cos \theta. \end{aligned} \quad (3.3-3)$$

The form of kinematic relations (3.3-1) and (3.3-3) is well suited to failure identification of the rate and attitude gyros in that the derivative of a variable is not written as a function of the variable itself.

1) *Attitude Sensor Failures:* Utilization of the rotational kinematics for failure identification of the attitude sensors is illustrated here by a detailed consideration of the roll attitude sensor. The other sensors can be considered in a similar fashion.

The predicted change in the roll angle over a time interval (t_{n-1}, t_n) can be obtained using a discrete approximation of (3.3-3):

$$\hat{\phi}(t_n) = \hat{\phi}(t_{n-1}) + \bar{p}_m [t_n - t_{n-1}] + [\psi_m(t_n) - \psi_m(t_{n-1})] \sin \bar{\theta}_m \quad (3.3-4)$$

where average measurements are used as before to minimize filter errors. The comparison of the measured roll angle and the predicted roll angle $\hat{\phi}'$ yields the residual

$$\gamma_\phi(t_n) = \phi_m(t_n) - \hat{\phi}'(t_n). \quad (3.3-5)$$

The residual γ_ϕ is used to update the estimate $\hat{\phi}$ using

$$\hat{\phi}(t_n) = \hat{\phi}'(t_n) + k \gamma_\phi(t_n) \quad (3.3-6)$$

where k represents a suitably chosen filter gain.

Equations (3.3-4)–(3.3-6) represent the roll filter. The pitch and yaw filter equations may be similarly obtained using (3.3-3). As in the translational kinematics filters, these rotational filters have been simplified in form to minimize computational complexity and to limit each failure signature to a single channel. This decoupling of the roll, pitch, and yaw channels is accomplished by using measurements, rather than estimates, of the Euler angles and body rates in the propagation equations [e.g., (3.3-4)].

As in the translational kinematics case, a conflict exists between the desire for noise suppression in normal operation and the desire for large observable failure signatures. The conflict was resolved in that case by using a single filter with appropriate nonzero gain k to initialize, after failure detection by the trigger, the two $k=0$ filters used by the SPRT's for failure identification. A similar implementation of (3.3-4)–(3.3-6) for failure identification of the attitude sensors will now be presented.

A nonzero value of k is chosen in (3.3-6) to give good filter perfor-

mance in the absence of failures by minimizing the effects of allowable noise on unfailed instruments. Two versions of the equations are implemented, each using a different roll attitude sensor to give ϕ_m . Each filter stores the last N residuals γ_ϕ from (3.3-5). It is assumed that there are less than N samples between the onset of an attitude sensor bias and its detection by the redundancy trigger. The signature of such a sensor bias in the residual decays exponentially at a rate proportional to the gain k , making it difficult to identify in the presence of noise. However if the gain is zero, the sensor bias failure signature is a step in the residual. This step persists in time, enhancing its identification. Therefore, at the time a roll attitude gyro failure is detected, calculations are made which effectively set $k=0$ for the two filters commencing N samples prior to the detection time. This is accomplished by using the stored $k \neq 0$ residuals via the relation

$$\gamma_{k=0}(t_n) = \gamma_{k \neq 0}(t_n) + k \sum_{\tau=t_d-N}^{t_n-1} \gamma_{k \neq 0}(\tau) \quad (3.3-7)$$

where t_d denotes the failure detection time. The $k=0$ residuals for each filter are the input to an SPRT looking for a bias in the filter's roll attitude gyro, where each SPRT mean has the predefined roll BFM and sign consistent with the output of the redundancy trigger.

Pairs of uncoupled filters similar to (3.3-4)–(3.3-6) are implemented for the pitch and yaw attitude sensors, and failure detection and identification for these sensors are accomplished in a manner identical to that described above for the roll attitude sensors.

The primary error sources in the $k=0$ residuals given by (3.3-4)–(3.3-6) are the acceptable biases on unfailed rate gyros which are integrated by the $k=0$ filters. In addition, another error source is the uncertainty in the orientation of the axes about which the body rates and Euler angle rates are measured. This axis uncertainty can arise from such factors as mounting errors, structural bending and attitude sensor errors. The magnitude of errors possible from this source should be considered when doing failure identification for the rotational sensors during high maneuver rates.

2) *Attitude Rate Sensor Failures:* As was done for attitude sensor failures, failure identification for the attitude rate sensors will be illustrated by considering only one instrument, the roll rate gyro. Analogous procedures are followed for the pitch and yaw rate gyros.

The predicted roll rate $p'(t_n)$ at the midpoint of the interval (t_{n-1}, t_n) is related to the attitude sensor measurements by the discrete approximation to the first equation of (3.3-1):

$$p'(t_n)[t_n - t_{n-1}] = [\phi_m(t_n) - \phi_m(t_{n-1})] - [\psi_m(t_n) - \psi_m(t_{n-1})] \sin \bar{\theta}_m \quad (3.3-8)$$

and the residual between the measured motion and the predicted motion is given by

$$\tilde{\gamma}_p(t_n) = [\bar{p}_m - p'(t_n)][t_n - t_{n-1}] \quad (3.3-9)$$

where again the overbar indicates a quantity averaged over the time interval. In order to minimize the effects of attitude measurement noise in the effective differentiation in (3.3-8), the residual γ_p is defined as

$$\gamma_p(t_n) = \sum_{\tau=t_d}^{t_n} \tilde{\gamma}_p(\tau) \quad (3.3-10)$$

where t_d is the time of roll rate gyro failure detection by the redundancy trigger. Since the summation operation in (3.3-10) follows the differencing in (3.3-8), the use of γ_p for failure identification removes the undesirable noise correlation in successive samples of $\tilde{\gamma}_p$. Two residual processes γ_p are formed after roll rate gyro failure detection, each one using a different roll rate gyro measurement. Each process γ_p constitutes the input to an SPRT looking for the effect of a bias failure in the corresponding roll rate gyro. The mean of each SPRT starts at zero and is incremented at each sample by a quantity whose magnitude is the predefined roll rate gyro BFM multiplied by the time step and whose sign is consistent with the output of the redundancy trigger.

The primary error source in failure identification for the attitude rate gyros via (3.3-8)-(3.3-10) and their analogs for the pitch and yaw rate gyros is Euler angle bias. This bias can arise from the acceptable biases on unfailed instruments or from axis misalignment, and its effect is proportional to vehicle maneuver rate.

D. Summary

In this section we outline three forms of analytic redundancy available on the F-8 DFBW aircraft and the use of SPRT's observing comparisons based on this analytic redundancy to identify bias failures for various sensor types. These SPRT's are quite simple in form, being either scalar or the sum of two scalars; and because of the information on the sign of the failure available from the redundancy trigger, only two SPRT's per instrument type are required for each form of analytic redundancy.

For each type of analytic redundancy SPRT, error sources have been enumerated and appropriate solutions to minimize their effects have been suggested. These solutions range from the active technique of clipping the gain on the translational kinematics SPRT's to suppress wind shear signatures to the passive technique of raising the assumed test error during violent aircraft maneuvers to account for the effects of alignment uncertainties on the rotational kinematics SPRT's.

At this time we will also mention a fourth type of analytic redundancy which has undergone only preliminary analysis to date. This is the redundancy which exists between the vertical position given by the altimeter output and the vertical position computed as the double integral of the compensated accelerometer and vertical gyro outputs. Although preliminary results indicate reliable identification of altimeter and normal accelerometer failures, detailed statements concerning the performance and limitations of these altitude kinematics SPRT's require further analysis.

IV. NUMERICAL RESULTS

In this section we present some representative results of the response of the redundancy trigger and the various direct and analytic redundancy SPRT's to sensor bias failures in the presence of measurement noise during a violent aircraft maneuver.

The simulated aircraft state time history is shown in Fig. 1. The aircraft is initially trimmed to horizontal flight at Mach 0.6 and 20000-ft altitude. After 1 s, step changes are made in the aileron, rudder, and elevator of +6, +6, and -8°, respectively. These new control surface positions are held for the remainder of the simulation. The violence of this maneuver is reflected by the 4-g peak in normal acceleration, 1-g peak in lateral acceleration and 2-rad/s peak in roll rate shown in the figure.

Table I indicates the 1-σ white noise levels and quantization sizes for the various sensor types. In addition, the RSS bias magnitudes for unfailed sensors are given where known. The simulation used the white noise and quantization values shown in the table, but no biases in the unfailed sensors were included.

Fig. 2 indicates the response of the relevant translational kinematics and dynamics SPRT's to a bias in the number 1 normal accelerometer of -6.4 ft/s² occurring at 1 s. The normal accelerometer BFM was defined to be the failure magnitude, 6.4 ft/s². The filter used for translational kinematics SPRT initialization had a time constant of 0.5 s. The sample periods for the filters and all SPRT's was 0.0625 s. The thresholds for the redundancy trigger and all SPRT's were chosen to give equal missed alarm and false alarm probabilities of 10⁻⁴. The translational dynamics SPRT used the same aerodynamic coefficient tables as used to compute the aircraft motion. Thus the only errors in the determination of the aerodynamic forces computed by the translational dynamics SPRT's were due to air data sensor noise. The variance of the translational kinematics SPRT was defined as 100 ft²/s² while the variance for the translational dynamics SPRT was defined as 100 ft²/s⁴. All of the SPRT outputs shown in Fig. 2 have been normalized by the threshold magnitude and truncated at unit magnitude; thus the failure threshold on these SPRT's is -1 and the no-failure threshold is +1.

At 1.3125 s, the redundancy trigger for the normal accelerometers detected the failure in its moving window average and indicated the sign of instrument 1 minus instrument 2 to be negative. At this time, five

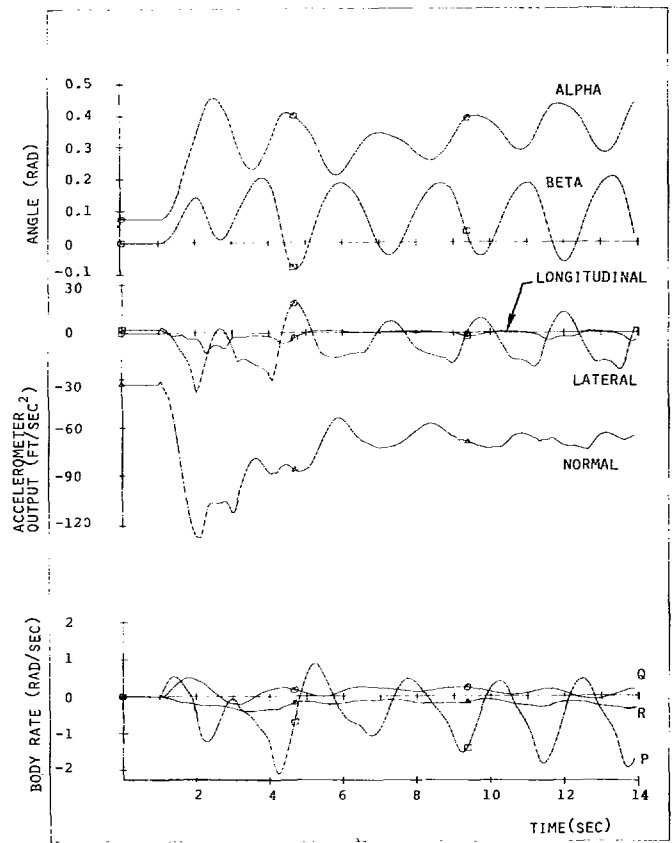


Fig. 1. Simulated aircraft state.

TABLE I
SENSOR INFORMATION

SENSOR TYPE	SIGMA	QUANTIZATION	RSS UNFAILED BIASES	UNITS
M	.01	.0056	—	%
α	.01	.00017	—	rad
a _x	1	.035	1.5	ft/sec ²
a _y	1	.035	1.5	ft/sec ²
a _z	1	.176	1.5	ft/sec ²
p	.0024	.0024	.01	rad/sec
q	.0007	.0007	.003	rad/sec
r	.0007	.0007	.003	rad/sec
δ	.01	.0015	—	rad
ε	.01	.0015	—	rad
ψ	.01	.0015	—	rad
h	.01	.00017	—	rad
h	10	11.1	—	ft

SPRT's were started: The direct redundancy SPRT, two k=0 translational kinematics SPRT's, and two translational dynamics SPRT's. The direct redundancy SPRT was looking for a mean of -6.4 ft/s² in the output of instrument 1 minus the output of instrument 2. One dynamics and one kinematics SPRT were looking for the effects of a -6.4 ft/s² bias in instrument 1, while the other dynamics and kinematics SPRT's were looking for the effects of a +6.4 ft/s² bias in instrument 2.

The first plot shows the direct redundancy SPRT crossing the failure threshold after one sample and remaining over the threshold for the rest

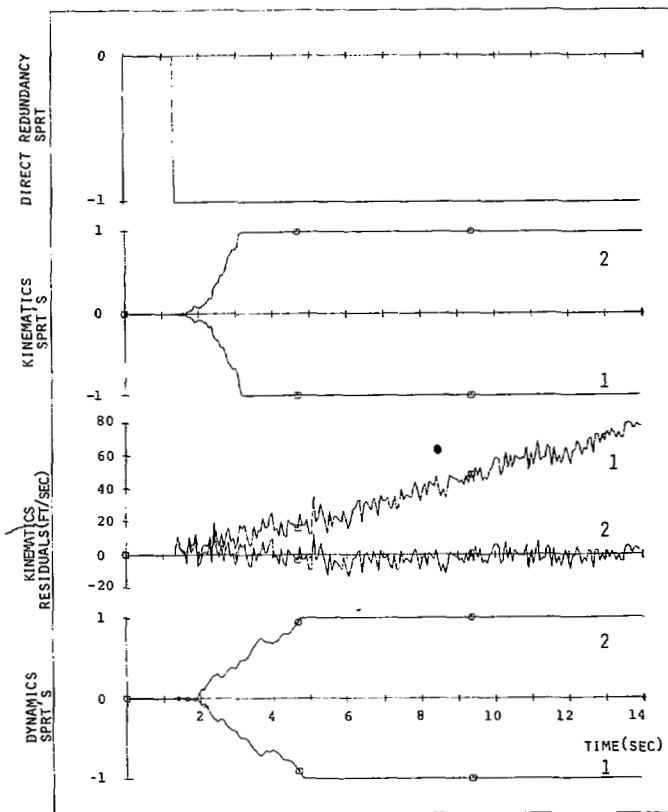


Fig. 2. Normal accelerometer number 1 bias failure at 1 s.

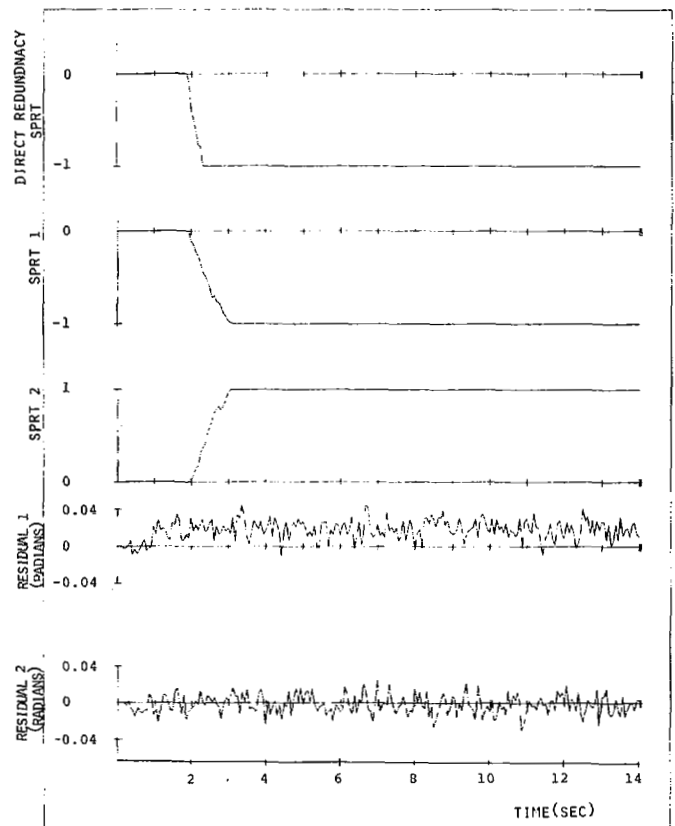


Fig. 3. Roll attitude gyro number 1 bias failure at 1 s.

of the simulation. The second set of plots shows the translational kinematics SPRT's while the third set of plots shows the $k=0$ filter residuals which are inputs to these SPRT's. As mentioned in Section III-A, the mean used in the $k=0$ translational kinematics SPRT is a ramp for an accelerometer bias failure. This ramp is clearly evident in the residual history for the filter using instrument 1 and absent from the residual history for the filter using instrument 2. The translational kinematics SPRT's reflect this residual behavior, with the SPRT looking for the effect of a negative bias in instrument 1 crossing the failure threshold at 3.1875 s and the SPRT looking for the effect of a positive bias in instrument 2 crossing the no-failure threshold at the same time. The fourth set of plots show the translational dynamics SPRT's looking for the effects of a negative bias in instrument 1 and a positive bias in instrument 2. These SPRT's cross the proper thresholds at about 4.75 s.

It is important to note that the plots of Fig. 2 indicate that the translational kinematics and dynamics SPRT's perform well in the presence of a rapidly changing aircraft state, implying that the second-order integration schemes described in Section III are sufficiently accurate.

Fig. 3 indicates the performance of the direct redundancy and rotational kinematics SPRT's to a bias in roll attitude gyro number 1 of 0.02 rad occurring at 1 s. The simulation includes the same measurement noises and maneuver mentioned above, with the addition of the 99-percent wind model mentioned in Section III-A. Again, there are no biases on unfailed sensors. The BFM for the roll attitude gyro was defined to be 0.02 rad. The variance used in the rotational kinematics SPRT's was 0.0004 rad^2 . The size of the moving window of residuals for the rotational kinematics filter was 1 s with a gain of 0.125 used before failure detection.

At 1.875 s, the roll attitude gyro redundancy trigger detects the failure and indicates that the sign of instrument 1 minus instrument 2 is positive. At this time the direct redundancy roll attitude gyro SPRT is initiated along with two rotational kinematics SPRT's, one looking for the effect of a positive bias in instrument 1 and the other looking for the effect of a negative bias in instrument 2. The outputs of these SPRT's are shown in plots one, two, and three, respectively. Plots four and five show

the $k=0$ filter residuals which form the inputs to the SPRT's shown in plots two and three, respectively. Plot four shows the characteristic bias occurring at 1 s in the residual for the $k=0$ filter using instrument 1, while plot five shows the absence of any bias in the residual for the filter using instrument 2. Consistent behavior is shown by the rotational kinematics SPRT's, with the SPRT looking for the effect of a positive bias in the instrument 1 crossing the failure threshold at 3.1875 s and the SPRT looking for the effect of a negative bias in instrument 2 crossing the no-failure threshold at the same time. The direct redundancy SPRT crosses the failure threshold at 2.25 s, corroborating the presence of a roll attitude gyro failure.

V. BFM SELECTION, THE QSPR, AND THE OUTER LOOP

The direct redundancy trigger and analytic redundancy SPRT's discussed in Section IV were chosen for illustrative purposes to be consistent only with the unfailed noise characteristics of the various sensors. However, the effects of allowable biases on unfailed instruments and the effects of maneuvers were ignored. In [22] we outline a technique for consistent BFM selection which accounts for the effects of biases in unfailed instruments. For each instrument type, we define a bias magnitude B for each type of analytic redundancy test. These B 's are chosen to avoid false alarms due to all effects, with maneuver-dependent terms evaluated at trim at Mach 0.6 at 20000-ft altitude. The *elapsed time limit* (ETL) for each instrument type-analytic redundancy combination is defined to be 1.5 times the required time for the SPRT of the failed sensor to cross the failure threshold using worst case errors at trim. The BFM for each instrument type is defined as the minimum value of B for all of the analytic redundancy tests available for that instrument type. The tests are designed, wherever possible, to detect bias failures of $B/\sqrt{2}$. Thus if we average the two instruments of a given type whenever they are needed in SPRT's for *other* instruments, we then have that the worst case RSS bias in this average is $\text{BFM}/2$, and this figure is used in the calculation of test errors for other instruments.

In [22] we also introduce the QSPR. In essence, the QSPR is the

output of an SPRT which assumes a bias failure of magnitude equal to the magnitude of the difference between the two suspect sensors, plus worst case RSS test errors in the sense opposite to the failure. In the QSPR, maneuver-dependent error sources are evaluated using actual averaged sensor output, *not* assuming trim as before. Thus the QSPR is a measure at every time sample of the signal-to-noise ratio of its associated analytic redundancy test. The way the QSPR is defined in [22], its negativity implies that the SPRT using the failed sensor *must* be lower than the SPRT using the unfailed sensor. With this in mind we have designed the following preliminary outer loop identification logic.

Following a direct redundancy trigger, for some instrument type, N_p passes are allowed through the logic, each pass equal in time to the longest ETL of all applicable analytic redundancy tests. If the trigger is not reconciled after N_p passes, an unidentifiable failure is announced, at which point the pilot may maneuver (or stop maneuvering) the aircraft to enhance failure identifiability. The trigger may be reconciled by a false alarm indication, in which the direct redundancy SPRT becomes positive, or by a failure identification. Failure identification checks are made at each time step using every applicable analytic redundancy QSPR and the associated instrument SPRT outputs. For each form of analytic redundancy, only the instrument with the smallest SPRT output, call it instrument j , is used. Now, assume the QSPR and SPRT outputs are normalized by the threshold magnitude. Then if the time t_n is before ETL of the test, instrument j is identified as failed if

$$QSPR_n < -1 \text{ and } u_n^j < -1.$$

If the time t_n is at or beyond ETL of the test, instrument j is identified as failed if

$$QSPR_n < -1 \text{ and } u_n^j < 0$$

or

$$QSPR_n < 0 \text{ and } u_n^j < -1.$$

Additionally, using appropriate redundancy tests, an instrument is *provisionally failed* if u_n^j and QSPR are negative but above the failure threshold. The provisionally failed instrument is removed from all control calculations, but the failure tests continue until the redundancy trigger is reconciled. This capability of the dual-redundant system to make provisional failures tends to minimize the time required to remove a failed sensor from the system without a corresponding increase in false identifications.

We point out that by incorporating the QSPR with its worst case possibilities into the identification logic, we are essentially building caution into the system. However, if there is a large failure, the QSPR will indicate the presence of a high signal-to-noise ratio, and a quick decision can be made. It is only in the case of small failures (or large noise) that the QSPR will correctly tell us to be more circumspect.

VI. CONCLUSIONS

In this paper, we have discussed a currently evolving technique for dual redundant sensor FDI for the NASA F-8 DFBW aircraft. The technique involves a dual mode procedure in which failure detection is accomplished by observing the difference between like instrument outputs, and failure identification is accomplished using the analytic redundancy available as functional relationships among the outputs of dissimilar instruments.

Various types of analytic redundancy present on the aircraft have been discussed, and the use of this analytic redundancy in designing SPRT's for failure identification for the various sensors has been detailed. It is emphasized that these SPRT's were designed to involve minimal computational complexity. SPRT error sources such as axis

misalignment, wind shear, and biases on unfailed sensors have been enumerated along with corresponding suggestions for minimizing their effects. Preliminary simulation results were presented which showed good SPRT performance during a violent maneuver in the absence of these error sources, indicating sufficient accuracy of the digital filter equations. However, determination of the performance of the algorithm in the presence of all error sources awaits extensive simulations planned for the future. We have discussed the QSPR and its utilization by a preliminary form of the outer loop identification logic. This outer loop uses provisional failure decisions, allowed by the dual sensor redundancy, to minimize identification time without corresponding increased false identification penalties.

Several additional areas of future investigation have been mentioned. Among these are the use of SPRT's to identify failures when no dual instrument redundancy is available, and identification of simultaneous failure of the roll and pitch outputs of a vertical gyro. We add here that an effort was recently completed to define the aerodynamic coefficients used in Section III-B as functions of the air data variables. This has resulted in a factor-of-eight decrease in required storage compared with the tables used in the reported simulations. These approximations produce errors in the translational dynamics SPRT's which are minimal in the most common flight regimes.

REFERENCES

- [1] A. S. Willsky, "A survey of design methods for failure detection in dynamic systems," *Automatica*, vol. 12, pp. 601-611.
- [2] R. V. Beard, "Failure accommodation in linear systems through self-reorganization," NASA, Rep. CR-118314, 1971.
- [3] H. L. Jones, "Failure detection in linear systems," Ph.D. dissertation, Dep. Aeronautics and Astronautics, M.I.T., Cambridge, MA, Sept. 1973.
- [4] J. Gilmore and R. McKern, "A redundant strapdown inertial reference unit (SIRU)," *J. Spacecraft and Rockets*, vol. 9, pp. 39-47, Jan. 1972.
- [5] R. B. Broen, "A nonlinear voter-estimator for redundant systems," in *Proc. 1974 IEEE Conf. on Decision and Control*, Phoenix, AZ, pp. 743-748.
- [6] R. C. Montgomery and A. K. Caglayan, "Failure accommodation in digital flight control systems by Bayesian decision theory," *J. Aircraft*, vol. 13, pp. 69-75, Feb. 1976.
- [7] A. S. Willsky, J. J. Deyst, Jr., and B. S. Crawford, "Two self-test methods applied to an inertial system problem," *J. Spacecraft and Rockets*, vol. 12, pp. 434-437, July 1975.
- [8] M. H. A. Davis, "The application of nonlinear filtering to fault detection in linear systems," *IEEE Trans. Automat. Contr.*, vol. AC-20, pp. 257-259, Apr. 1975.
- [9] T. T. Chien, "An adaptive technique for a redundant-sensor navigation system," Charles Stark Draper Lab., Inc., Cambridge, MA, Rep. T-560, Feb. 1972.
- [10] T. H. Kerr, "A two ellipsoid overlap test for real time failure detection and isolation by confidence regions," presented at the Pittsburgh Conf. on Modeling and Simulation, Apr. 24-26, 1974.
- [11] R. K. Mehra and J. Peschon, "An innovations approach to fault detection and diagnosis in dynamic systems," *Automatica*, vol. 7, pp. 637-640.
- [12] A. S. Willsky and H. L. Jones, "A generalized likelihood ratio approach to the detection and estimation of jumps in linear systems," *IEEE Trans. Automat. Contr.*, vol. AC-21, pp. 108-112, Feb. 1976.
- [13] J. J. Deyst and J. C. Deckert, "Maximum likelihood failure detection techniques applied to the shuttle RCS jets," *J. Spacecraft and Rockets*, vol. 13, pp. 65-74, Feb. 1976.
- [14] P. Sanyal and C. N. Shen, "Bayes' decision rule for rapid detection and adaptive estimation scheme with space applications," *IEEE Trans. Automat. Contr.*, vol. AC-19, pp. 228-231, June 1974.
- [15] R. N. Clark, D. C. Fosth, and V. M. Walton, "Detecting instrument malfunctions in control systems," *IEEE Trans. Aerosp. Electron. Syst.*, vol. AES-11, pp. 465-473, July 1975.
- [16] P. M. Newbold and Y.-C. Ho, "Detection of changes in the characteristics of a Gauss-Markov process," *IEEE Trans. Aerosp. Electron. Syst.*, vol. AES-4, pp. 707-718, Sept. 1968.
- [17] A. Wald, *Sequential Analysis*. New York: Wiley, 1947, ch. 3.
- [18] K. Fukunaga, *Introduction to Statistical Pattern Recognition*. New York: Academic, 1972, pp. 77-84.
- [19] A. H. Jazwinski, *Stochastic Processes and Filtering Theory*. New York: Academic, 1970, ch. 8.3.
- [20] J. C. Houbolt, R. Steiner, and K. G. Pratt, "Dynamic response of airplanes in atmospheric turbulence including flight data on input and response," NASA TR R-199, 1964.
- [21] R. L. Halfman, *Dynamics*, vol. 1. Reading, MA: Addison-Wesley, 1962, p. 200.
- [22] J. C. Deckert, M. N. Desai, J. J. Deyst, and A. S. Willsky, "A reliable dual-redundant sensor FDI system for the NASA F8C-DFBW aircraft," in *Proc. 1976 IEEE Conf. on Decision and Control*, Clearwater Beach, FL, Dec. 1976, pp. 32-37.
- [23] M. N. Desai, J. C. Deckert, J. J. Deyst, A. S. Willsky, and E. Y. Chow, "Dual redundant sensor FDI techniques applied to the NASA F8C-DFBW aircraft," in *Proc. AIAA Guidance and Control Conf.*, San Diego, CA, Aug. 1976, pp. 502-513.